J Mater Sci: Mater Electron (2020) 31:21813–21819

Effect of vacuum annealing and heating–cooling cycle annealing on the soft magnetic properties at room- and high-temperatures for nanocrystalline FeCoAlSiBCuNb alloy

Qian-qian Hao[1], Zhi Wang[1,*], Yan Zhang[1], Xian-hua Li[1], and Rui-min Shi[2]

[1] School of Science, Tianjin University, Tianjin 300072, People's Republic of China
[2] School of Mathematics and Physics, Handan College, Handan 056005, People's Republic of China

Received: 1 August 2020
Accepted: 15 October 2020
Published online: 26 October 2020

ABSTRACT

Effect of vacuum annealing and heating–cooling cycle annealing on the soft magnetic properties at room- and high-temperatures for $(Fe_{0.9}Co_{0.1})_{72.7}Al_{0.8}Si_{13.5}B_9Cu_1Nb_3$ alloy was investigated by the temperature dependence of initial permeability (μ_i-T curves). The crystallization behavior and microstructural evolution of alloy with the increase of annealing temperature were studied by means of differential scanning calorimeter (DSC) and X-ray diffraction (XRD). After vacuum annealing at 617 °C for 0.5 h, the μ_i can reach 30,300 and maintain more than 1000 until 640 °C because of larger crystalline volume fraction (V_{cry}) of 81.9% and smaller intergranular amorphous layer (Λ) of 0.930 nm, which is more excellent than that of other Fe–Co–Al–Si–B–Cu–Nb alloys annealed at their optimum temperatures. In addition, the crystallized interval temperature (ΔT_x) of 158 °C, superior to $Fe_{73.5}Si_{13.5}B_9Nb_3Cu_1$ and $(Fe_{0.9}Co_{0.1})_{73.5}Si_{13.5}B_9Nb_3Cu_1$ alloys ever reported, is conducive to precipitating the bcc α-(Fe,Co,Si) and Fe_3(Si,Co,Al) soft magnetic crystalline phases and improving thermostability of alloy.

1 Introduction

Magnetism, one of the most basic physical properties, is ubiquitous among various substances. As indispensable functional materials in various fields, a variety of magnetic materials not only meet the development requirements of traditional industries, but also play an increasingly important role in high-tech fields such as power, electronics and communications. The soft magnetic material is one of the most typical magnetic materials, having excellent comprehensive soft magnetic properties including high saturation magnetization (M_s), high permeability (μ_i), low coercivity (H_c) and low loss (W) etc. [1], which

Address correspondence to E-mail: zhiwang@tju.edu.cn

https://doi.org/10.1007/s10854-020-04693-w

meets the needs of the era of green, energy saving, environmental protection and high efficiency. What's more, typical Fe-based alloys are widely used in communication, computer and other high-tech fields as a result of the high initial permeability at room temperature. However, relatively low Curie temperature of amorphous phase (T_c^{am}) and crystallized interval temperature (ΔT_x) limited the application of the alloys at high temperature [2, 3]. Some studies found that the adulteration of moderate Co increased both the ΔT_x and the T_c^{am}, which was beneficial to form the single soft magnetic phase and improve the thermostability of the alloys [4–6]. And adding moderate Al to FeCo-based alloy obtained larger ΔT_x above 210 °C [7, 8] and higher T_c^{am} than that of typical $Fe_{73.5}Si_{13.5}B_9Cu_1Nb_3$ alloys [3]. Therefore, the nanocrystalline $(Fe_{0.9}Co_{0.1})_{72.7}Al_{0.8}Si_{13.5}B_9Cu_1Nb_3$ alloy after vacuum annealing and heating–cooling cycle annealing was studied in this paper.

We mainly analyzed the changes of μ_i-T curves by XRD patterns, Herzer's Model and magnetic coupling, and further explored the relationship between microstructure and soft magnetic properties in order to find optimal magnetic softness at room and high temperatures.

2 Experimental procedures

First, the smelted spindle was made into a series of amorphous ribbons with the width of 2 mm and thickness of 20 μm by the single-roller melt-spinning technique, some of which were winded into toroidal cores with the outer diameter of 18 mm and inner diameter of 16 mm for cycle annealing and vacuum annealing, some of which were cut up for the thermal analysis of differential scanning calorimeter (DSC) using NETZSCH STA 409 PC/PG from room temperature to 1000 °C at a heating rate of 10 K/min. Next, the μ_i-T curves of samples after different thermal treatment were measured in a furnace with Ar atmosphere protection in order to observe the temperature dependence of initial permeability by an HP4294A impedance analyzer at $H = 0.4$A/m and $f = 10$ kHz. Finally, the characterization of microstructure was obtained by X-ray diffraction (XRD) using D/max-2500/PC with Cu-K$_\alpha$ radiation (λ = 1.54056 Å) to analyze the relations between the microstructure and soft magnetic properties of the alloys after vacuum annealing at 500–660 °C for 0.5 h (Fig. 1).

3 Results and discussion

The DSC curves of as-quenched $(Fe_{0.9}Co_{0.1})_{72.7}Al_{0.8}Si_{13.5}B_9Cu_1Nb_3$ alloys show two separated exothermic peaks related to the enthalpy change and exothermic phase transformations [9, 10], the endothermic peak is corresponding to the melting of ribbons over the temperature range from 480 to 510 °C [11]. The onset primary crystallization temperature T_{x1} corresponds to the formation of crystalline α-Fe(Co,Si) and Fe_3(Si,Co,Al) phase shown in Fig. 2b, while the onset temperature of second crystallization T_{x2} relates to final crystallization of boride Fe_2B [12], the temperature interval ΔT_x ($\Delta T_x = T_{x2} - T_{x1}$) of 158 °C is superior to that of $Fe_{73.5}Si_{13.5}B_9Nb_3Cu_1$ [2] and $(Fe_{0.9}Co_{0.1})_{73.5}Si_{13.5}B_9Nb_3Cu_1$ alloys [13], which is beneficial to obtain the single crystalline phase. It is well known that the size of particle relates to annealing temperature [14], higher annealing temperature leads to larger average grain size and crystalline volume fraction [15–18], which is substantiated in Table 1.

Figure 2 shows the XRD patterns of as-quenched and annealed $(Fe_{0.9}Co_{0.1})_{72.7}Al_{0.8}Si_{13.5}B_9Cu_1Nb_3$ alloy. It can be seen that the diffraction peak of as-quenched alloy is one broad scattering peak at around $2\theta = 45°$,

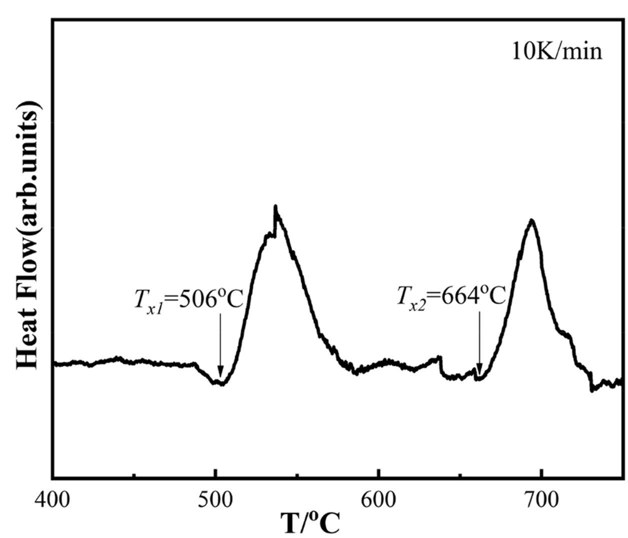

Fig. 1 DSC curve of as-quenched $(Fe_{0.9}Co_{0.1})_{72.7}Al_{0.8}Si_{13.5}B_9Cu_1Nb_3$ alloys at a heating rate of 10 K/min

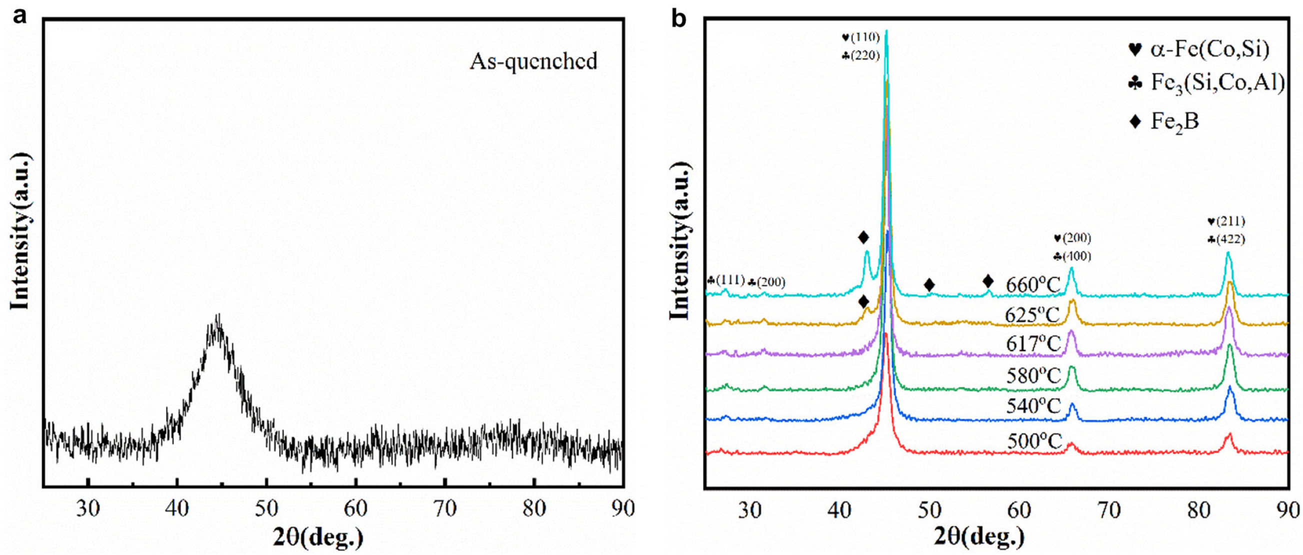

Fig. 2 XRD patterns of $(Fe_{0.9}Co_{0.1})_{72.7}Al_{0.8}Si_{13.5}B_9Cu_1Nb_3$ alloy as-quenched (**a**) and annealed at 500–660 °C for 0.5 h (**b**)

indicating that the as-quenched sample is complete amorphous state [19]. After vacuum annealing at 500–617 °C, the samples show the characteristic (110), (200) and (211) diffraction peaks of bcc α-(Fe,Co,Si) crystalline phase and the characteristic (111), (200), (220), (400) and (422) diffraction peaks of Fe_3(-Si,Co,Al) crystalline phase, which suggests that the annealed samples are partially crystallized and form the desired two-phase nanocrystalline structure related to the crystallization phase and remaining amorphous phase.

The volume fraction of crystallization phase V_{cry} can be estimated by XRD spectra as follows [20]:

$$V_{cry} = \frac{I_{cry}}{I_{cry} + KI_{am}} \quad (1)$$

where I_{cry} and I_{am} denote the integral intensities of diffraction peaks of crystalline phase and amorphous phase respectively. K is a constant determined by experiment. With the increase of annealing temperature (T_a), the V_{cry} gradually increases from 77.3% for T_a=500 °C to 81.9% for T_a = 617 °C shown in Table 1. According to the full width at half maximum (FWHM) of the (110) and (220) diffraction peaks, the theoretical Scherrer formula [21–25] is used to calculate the average grain size (D):

$$D = \frac{K\lambda}{\beta \cos\theta} \quad (2)$$

where 'K', 'λ', 'β' and 'θ' are the Scherrer constant (K is nealy 1) [18, 26], wavelength of Cu-Kα radiation (λ = 1.54056 Å), the full width at half-maximum height (FWHM) and the Bragg diffraction angle, respectively. The results showed that the D gradually increases from 11.5 to 13.5 nm with the increase of T_a shown in Table 1. According to the V_{cry} and D, the thickness of amorphous layer (Λ) is calculated as follows [27]:

$$\Lambda = D\left[\left(\frac{1}{V_{cry}}\right)^{1/3} - 1\right] \quad (3)$$

The calculation results show that the Λ decreases from 1.032 nm for T_a = 500 °C to 0.930 nm for T_a = 617 °C, the higher V_{cry} and the thinner Λ can ensure the penetrating effect of strong exchange coupling between grains [13, 15, 17] and improve the soft magnetic properties of the alloy according to Hernando's model [27].

Therefore, The 617 °C-annealed (Fe0.9Co0.1)72.7Al0.8Si13.5B9Cu1Nb3 alloy with

Table 1 The average grain size D(nm), crystalline volume fraction (V_{cry}) and intergranular amorphous layer (Λ) of $(Fe_{0.9}Co_{0.1})_{72.7}Al_{0.8}Si_{13.5}B_9Cu_1Nb_3$ alloy annealed at 500–660 °C

T_a/°C	D/nm	V_{cry}/%	Λ/nm
500	11.5 ± 0.5	77.3 ± 0.5	1.032 ± 0.08
540	12.5 ± 0.5	78.2 ± 0.3	1.068 ± 0.06
580	13.5 ± 0.5	81.0 ± 0.3	0.983 ± 0.06
617	13.5 ± 0.5	81.9 ± 0.3	0.930 ± 0.06

larger V_{cry} of 81.9% and thiner Λ of 0.930 nm exhibits superior soft magnetic properties, which is verified in Fig. 3b.

Figure 3a shows the μ_i-T curve of as-quenched $(Fe_{0.9}Co_{0.1})_{72.7}Al_{0.8}Si_{13.5}B_9Cu_1Nb_3$ alloy. Amorphous structure with a sharp Hopkinson peak was observed near the Curie temperature of the amorphous phase T_c^{am} due to the faster decrease of magnetic anisotropy than that of the saturation magnetization when the temperature approaches T_c^{am} [28]. The μ_i abruptly drops to zero just above T_c^{am} due to ferro-paramagnetic transition of the amorphous alloy [13]. The μ_i rapidly rises from 0 to 2000 above 500 °C because of the precipitation of bcc α-(Fe,Co,Si) and Fe_3(Si,Co,Al) crystalline phases and it fleetly declines to zero at about 650 °C due to the precipitation of Fe_2B hard magnetic phase, which is consistent with the results of DSC curve.

The μ_i at room temperature increases greatly with the increase of the annealing temperature from 8400 for T_a = 500 °C to 30,300 for T_a = 617 °C. When T_a is 500 °C and 540 °C, the μ_i tends to decrease rapidly around T_c^{am}, which can be interpreted by Herzer's model [29]:

$$\langle K\rangle = \frac{1}{\phi^6}(1-V_{am})^4 K_1^4 D^6 \left[\frac{1}{\sqrt{A_{cr}}} + \frac{(1-V_{am})^{-1/3}-1}{\sqrt{A_{am}}}\right]^6 \quad (4)$$

$$\mu_i = P_\mu \frac{J_s^2}{\mu_0 \langle K\rangle} \quad (5)$$

where φ, A_{cr}, A_{am}, K_1, V_{am}, $<K>$, p_μ, μ_0 and J_s represent the spin rotation angle over the exchange–correlation length, exchange stiffness of crystalline phases, exchange stiffness of amorphous phases, magnetocrystalline anisotropy, amorphous volume fraction, effective magnetic anisotropy, a dimensionless prefactor, vacuum magnetic permeability and average saturation magnetic polarization respectively. In the dual-phase nanostructure, A_{am} drops to a much smaller value than A_{cr} when the temperature approaches to the T_c^{am} [30], which makes $<K>$ increase and μ_i decrease rapidly. While the increasing rate of $<K>$ is much slower at higher V_{cry}, showing the smoother decreasing rate of μ_i at higher T_a [31] such as annealing at 580 °C and 617 °C.

With further increasing annealing temperature from 625 to 660 °C, the initial permeability at room temperature decreases significantly from 3500 down to nearly zero due to the successive precipitating Fe_2B hard magnetic phase from amorphous matrix and the higher magnetocrystalline anisotropy of Fe-borides at room temperature [16]. But the μ_i of 625 °C-annealed sample gradually increases to 19,300 around 150 °C, and then decreases significantly with temperature further increasing. The μ_i peak may correspond to the minimum value of magnetocrystalline anisotropy for Fe_2B hard magnetic phase [16].

In conclusion, although 625 °C-annealed sample has a small amount of hard magnetic phase, there are few effects on the high-temperature magnetic

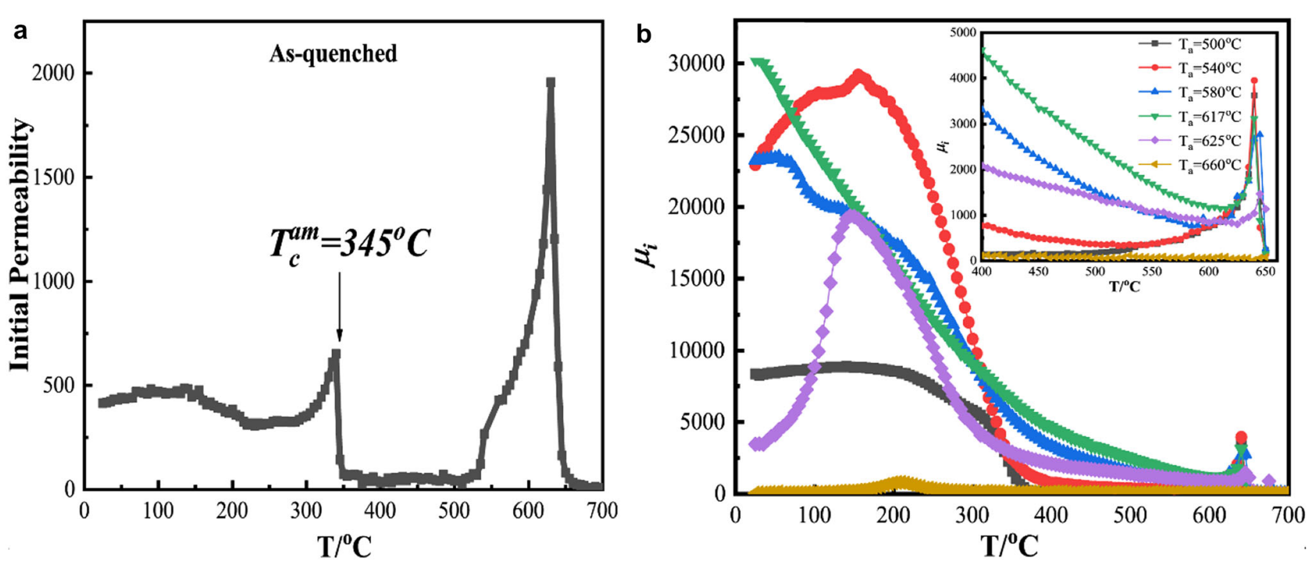

Fig. 3 μ_i-T curves of $(Fe_{0.9}Co_{0.1})_{72.7}Al_{0.8}Si_{13.5}B_9Cu_1Nb_3$ alloy as-quenched (**a**) and annealed at 500–660 °C (**b**)

Table 2 The initial permeability at room and high temperatures for Fe–Co–Al–Si–B–Cu–Nb alloys annealed at their optimal temperatures and conditions

Composition	Conditions	μ_{i25}	μ_{i500}	μ_{i550}	μ_{i600}
$(Fe_{0.5}Co_{0.5})_{73.5}Al_{0.6}Si_{13.5}B_{8.4}Cu_1Nb_3$ [8]	Vacuum annealing at 600 °C	1150	1100	1100	1100
$(Fe_{0.5}Co_{0.5})_{72.7}Al_{0.8}Si_{17.5}B_5Cu_1Nb_3$ [17]	Heating–cooling cycle annealing at 550 °C	1600	1500	1500	1500
$(Fe_{0.8}Co_{0.2})_{72.7}Al_{0.8}Si_{17.5}B_5Cu_1Nb_3$ [32]	Vacuum annealing at 640 °C	8100	2000	1500	500
$(Fe_{0.9}Co_{0.1})_{72.7}Al_{0.8}Si_{13.5}B_9Cu_1Nb_3$	Vacuum annealing at 617 °C	30,300	2500	1700	1200

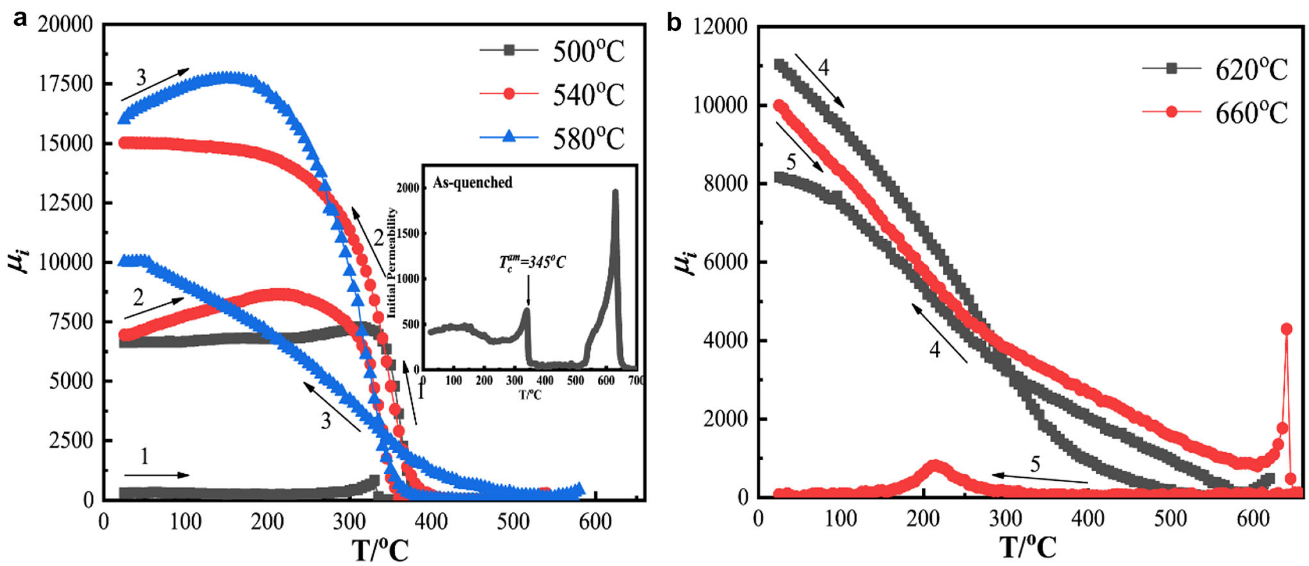

Fig. 4 μ_i-T curves of $(Fe_{0.9}Co_{0.1})_{72.7}Al_{0.8}Si_{13.5}B_9Cu_1Nb_3$ alloy during continuous heating–cooling cycle annealing at 500–660 °C for 15 min (the top temperature of each cycle is 500 °C, 540 °C, 580 °C, 620 °C and 660 °C repectively)

softness shown in partially enlarged inset of Fig. 3. The reason should be attributed to stronger magnetic coupling between grains for nanocrystalline alloys at higher T_a. What is more, the $(Fe_{0.9}Co_{0.1})_{72.7}Al_{0.8}Si_{13.5}B_9Cu_1Nb_3$ alloy has the highest μ_i of 30,300 and higher μ_i above 1000 until to 640 °C after optimal vacuum annealing at 617 °C, which is superior to other Fe–Co–Al–Si–B–Cu–Nb alloys in Table 2.

Table 2 shows the initial permeability of different Fe–Co–Al–Si–B–Cu–Nb alloys at 25 °C, 500 °C, 550 °C and 600 °C named as μ_{i25}, μ_{i500}, μ_{i550} and μ_{i600} to compare their magnetic softness at room- and high-temperatures. The results point out that the room-temperature initial permeability of $(Fe_{0.9}Co_{0.1})_{72.7}Al_{0.8}Si_{13.5}B_9Cu_1Nb_3$ alloy is distinctly higher than that of other alloys, and the high-temperature initial permeability at 500–600 °C is clearly superior to others except $(Fe_{0.5}Co_{0.5})_{72.7}Al_{0.8}Si_{17.5}B_5Cu_1Nb_3$ alloy at 600 °C. In summary, the $(Fe_{0.9}Co_{0.1})_{72.7}Al_{0.8}Si_{13.5}B_9Cu_1Nb_3$ alloy after vacuum annealing at 617 °C has more excellent magnetic softness at room and high temperatures than other Fe–Co–Al–Si–B–Cu–Nb alloys annealed at their optimal temperatures and conditions.

The μ_i-T curves of $(Fe_{0.9}Co_{0.1})_{72.7}Al_{0.8}Si_{13.5}B_9Cu_1Nb_3$ alloy during continuous heating–cooling cycle annealing at 500–660 °C are showed in Fig. 4. The shape of μ_i-T curves is related to phase structure of the alloys. A sharp Hopkinson peak appears at T_c^{am} for as-quenched alloy shown in enlarged inset of Fig. 4a. The cooling curve of 580 °C and vacuum annealing at same temperature have the same trend, the Hopkinson peak disappears and a higher μ_i is observed due to the formation of two-phase nanocrystalline structure [33]. In the fifth cycle, the alloy exhibited improved high-temperature magnetic softness during heating curve, the higher μ_i

above 1000 can keep up to 600 °C as a result of stronger magnetic coupling, and a sharp Hopkinson peak appears near 640 °C relating to the Curie temperature of crystalline phase. However, the μ_i is very low nearly zero shown in cooling curve of 660 °C as a result of precipitating the hard magnetic phase.

4 Conclusion

Effect of vacuum annealing and heating–cooling cycle annealing on microstructure and soft magnetic properties of nanocrystalline $(Fe_{0.9}Co_{0.1})_{72.7}Al_{0.8}Si_{13.5}B_9Cu_1Nb_3$ alloy was investigated. With the increase of vacuum annealing temperature from 500 to 617 °C, the V_{cry} gradually increases from 77.3 to 81.9% and the Λ decreases from 1.032 to 0.930 nm, which is conducive to enhancing the exchange coupling between magnetic particles and improving the soft magnetic properties. So 617 °C-annealed sample shows more excellent magnetic softness at room- and high-temperatures than that of other Fe–Co–Al–Si–B–Cu–Nb alloys ever reported. Furthermore, the variational trends of μ_i-T curves after cyclic annealing also exhibited that the excellent high-temperature magnetic softness was obtained by annealing around 620 °C.

Acknowledgements

This work was supported by the National Natural Science Foundation of China (under Grant No. 51271130).

References

1. M.E. McHenry, M.A. Willard, D.E. Laughlin, Amorphous and nanocrystalline materials for applications as soft magnets. Prog. Mater. Sci. **44**, 291–433 (1999)
2. T.H. Noh, M.B. Lee, H.J. Kim, I.K. Kang, Relationship between crystallization process and magnetic properties of Fe-(Cu-Nb)-Si-B amorphous alloys. J. Appl. Phys. **67**, 5568 (1990)
3. Y. Jia, Z. Wang, F. Wang, L. Zhang, H. Duan, Effect of Ti on structure and soft magnetic properties of Si-rich Finemet-type nanocrystalline $Fe_{73.5}Cu_1Nb_{3-x}Si_{17.5}B_5Ti_x$ alloys. Mater. Res. Bull. **106**, 296–300 (2018)
4. L.-X. Wen, Z. Wang, J. Wang, H. Zhang, High temperature magnetic permeability of Si-rich Finemet-type nanocrystalline $(Fe_{1-x}Co_x)_{74.5}Nb_2Si_{17.5}B_5Cu_1$ alloys. J. Magn. Magn. Mater. **379**, 265–269 (2015)
5. L. Xue, W. Yang, H. Liu, H. Men, A. Wang, C. Chang, B. Shen, Effect of Co addition on the magnetic properties and microstructure of FeNbBCu nanocrystalline alloys. J. Magn. Magn. Mater. **419**, 198–201 (2016)
6. Y.-M. Han, Z. Wang, X.-H. Che, X.-G. Chen, W.-R. Li, Y.-L. Li, Influence of Co content on the structure and magnetic permeability of nanocrystalline $(Fe_{1-x}Co_x)_{73.5}Cu_1Nb_3Si_{13.5}B_9$ alloys. Mater. Sci. Eng. B **156**, 57–61 (2009)
7. Y. Han, Z. Wang, Y.-C. Xu, Z.-Y. Xie, L.-J. Li, Influence of Al addition on structure and magnetic properties of nanocrystalline $Fe_{65}Co_{15}Si_5Nb_3Cu_1B_{11-x}Al_x$ alloys. J. Non-Cryst. Solids **442**, 29–33 (2016)
8. X.-H. Li, Z. Wang, H.-J. Duan, The effect of the minor Al addition on microstructure and soft magnetic properties for $(Fe_{0.5}Co_{0.5})_{73.5}Si_{13.5}Nb_3Cu_1B_9$ nanocrystalline alloy. J. Non-Cryst. Solids **517**, 114–118 (2019)
9. M. Yan, H. Tong, S. Tao, J. Liu, Structural and magnetic properties of $Fe_{73.5}Cu_1Nb_{3-x}Ti_xSi_{13.5}B_9$ ($x \leq 3$) alloys. J. Alloys Compd. **505**, 264–267 (2010)
10. D. Dastan, Effect of preparation methods on the properties of titania nanoparticles: solvothermal versus sol–gel. Appl. Phys. A **123**, 699 (2017)
11. Q. Zhu, Z. Chen, S. Zhang, Q. Li, Y. Jiang, P. Wu, K. Zhang, Crystallization progress and soft magnetic properties of FeGaBNbCu alloys. J. Magn. Magn. Mater. **475**, 88–92 (2019)
12. R. Brzozowski, M. Wasiak, H. Piekarski, P. Sovak, P. Uznanski, M.E. Moneta, Properties of Mn-doped FINEMET. J. Alloys Compd. **470**, 5–11 (2009)
13. L. Zhang, Z. Wang, Y.-R. Jia, Microstructure and soft magnetic properties of $(Fe_{0.9}Co_{0.1})_{73.5}Si_{13.5}B_{9-x}Nb_3Cu_1Ge_x$ nanocrystalline alloys. Mater. Sci. Eng. B **231**, 1–4 (2018)
14. D. Dastan, N. Chaure, M. Kartha, Surfactants assisted solvothermal derived titania nanoparticles: synthesis and simulation. J. Mater. Sci.: Mater. Electron. **28**, 7784–7796 (2017)
15. X. Ma, Z. Wang, X. Han, X. Yin, B. Wang, Microstructure and high-temperature soft magnetic properties of nanocrystalline $(Fe_{0.65}Co_{0.35})_{78.4}Si_9B_9Nb_{2.6}Cu_1$ alloy. Mater. Sci. Eng. A **448**, 216–220 (2007)
16. Z. Wang, K.Y. He, J. Jin, J. He, L. Zhang, H.W. Zhang, B.G. Shen, Temperature dependence of permeability for Fe–Cu–M–Si–B alloys. J. Mater. Sci. Eng. A **304–306**, 1046 (2001)
17. Y. Han, Z. Wang, Excellent high-temperature magnetic softness in a wide temperature for FeCo-based nanocrystalline alloy. J. Non-Cryst. Solids **434**, 92–95 (2016)
18. Z.-Y. Xie, Z. Wang, Y. Han, F.-F. Han, Influence of Ge on crystallization kinetics, microstructure and high-temperature

magnetic properties of Si-rich nanocrystalline FeAlSiB-CuNbGe alloy. J. Non-Cryst. Solids **463**, 1–5 (2017)
19. H. Duan, Z. Wang, Z. Xie, Y. Jia, Superior high-temperature magnetic softness for Co and Ge doped nanocrystalline $Fe_{72.7}Al_{0.8}Si_{17.5}B_5Cu_1Nb_3$ alloys. J. Magn. Magn. Mater. **460**, 495–500 (2018)
20. X.Y. Zhang, F.X. Zhang, J.W. Zhang, W. Yu, M. Zhang, J.H. Zhao, R.P. Liu, Y.F. Xu, W.K. Wang, Influence of pressures on the crystallization process of an amorphous alloy. J. Appl. Phys. **84**, 1918 (1998)
21. D. Dastan, P.U. Londhe, N.B. Chaure, Characterization of TiO_2 nanoparticles prepared using different surfactants by sol–gel method. J. Mater. Sci.: Mater. Electron. **25**, 3473–3479 (2014)
22. W.-D. Zhou, D. Dastan, J. Li, X.-T. Yin, Q. Wang, Discriminable sensing response behavior to homogeneous gases based on n-ZnO/p-NiO composites. Nanomaterials **10**, 785 (2020)
23. A. Jafari, K. Tahani, D. Dastan, S. Asgary, Z. Shi, X.-T. Yin, W.-D. Zhou, H. Garmestani, Ş Ţălu, Ion implantation of copper oxide thin films; statistical and experimental results. Surf. Interfaces **18**, 100463 (2020)
24. A. Jafari, M.H. Alam, D. Dastan, S. Ziakhodadadian, Z. Shi, H. Garmestani, A.S. Weidenbach, Ş Ţălu, Statistical, morphological, and corrosion behavior of PECVD derived cobalt oxide thin flms. J. Mater. Sci.: Mater. Electron. **30**, 21185–21198 (2019)
25. X.T. Yin, W.D. Zhou, J. Li, P. Lv, Q. Wang, D. Wang, F.Y. Wu, D. Dastan, H. Garmestani, Z. Shi, Ş Ţălu, Tin dioxide nanoparticles with high sensitivity and selectivity for gas sensors at sub-ppm level of hydrogen gas detection. J. Mater. Sci.: Mater. Electron. **30**, 14687–14694 (2019)
26. V. Uvarov, I. Popov, Metrological characterization of X-ray diffraction methods for determination of crystallite size in nano-scale materials. Mater. Charact. **58**, 883–891 (2007)
27. A. Hernando, I. Navarro, P. Gorria, Iron exchange-field penetration into the amorphous interphase of nanocrystalline materials. Phys. Rev. B **51**, 3281 (1995)
28. Y.Y. Jia, Z. Wang, J. Wang, R.M. Shi, Structure and magnetic properties of $Ni_5(Fe_{0.5}Co_{0.5})_{68.5}Si_{13.5}Nb_3B_9Cu$ alloy. J. Magn. Magn. Mater. **324**, 3981–3985 (2012)
29. G. Herzer, Grain size dependence of coercivity and permeability in nanocrystalline ferromagnets. IEEE Trans. Magn. **26**, 1397–1402 (2002)
30. Y.R. Jia, Z. Wang, F. Wang, Y. Han, Z.Y. Xie, L.J. Li, L. Zhang, Effect of P substitution for Nb on structure and soft magnetic properties of Si-rich FeCuNbSiB nanocrystalline alloys. Mater. Sci. Eng. B **222**, 55–59 (2017)
31. Y. Han, Z. Wang, L.X. Wen, Y.C. Xu, Excellent magnetic softness at room and high temperatures for Si-rich Fe-based nanocrystalline alloy with a small amount of Al. IEEE Trans. Magn. **51**, 2003704 (2015)
32. X.H. Li, Z. Wang, H.J. Duan, Effect of the partial substitution of FeCo by Ge on the magnetic properties of nanocrystalline $(Fe_{0.8}Co_{0.2})_{72.7}Al_{0.8}Si_{17.5}Nb_3Cu_1B_5$ alloy. J. Non-Cryst. Solids **522**, 119555 (2019)
33. L. Li, Z. Wang, Y. Han, Effect of Mo addition on high-temperature soft magnetic properties for air annealed FeCo-based nanocrystalline alloys. Mater. Lett. **185**, 235–238 (2016)